Defence Science Journal, Vol. 74, No. 5, September 2024, pp. 701-712, DOI : 10.14429/dsj.74.19737

Investigations on Penta Band High Isolation MIMO Antenna for 5G NR Bands and HIPERLAN Applications Using TCMA

Makkapati Himaja* and S. Yuvaraj

Department of Electronics and Communication Engineering, National Institute of Technology Andhra Pradesh, Tadepalligudem - 534 101, India

**E-mail: makkapati.himaja94@gmail.com*

ABSTRACT

The present article proposes a penta band Multiple Input Multiple Output (MIMO) antenna for 5G New Radio (NR) bands and HIPERLAN applications using Characteristic Mode Analysis (CMA). The design is obtained and optimised in step-by-step procedure using novel CMA approach and by perturbing the conventional rectangular structure with slots on the patch (left and right sides) and the ground plane (wide slot + narrow slots) for enhancing the isolation at multi bands. The MIMO configuration has a total dimension of 0.58 $\lambda_0 \times 0.35\ \lambda_0 \times 0.01\ \lambda_0$ mm^3 with an optimum element separation of 0.05 λ_0 (λ_0 is the lowest frequency operating wavelength). Multiband resonance is produced at 2.2, 4.2, 7.2, 16, 17.5 GHz. The radiating elements can excite various characteristic modes that support wider bandwidth. The -10 dB impedance bandwidth at working region are 0.2, 0.2, 0.38, 3.6, 2 GHz respectively. The suggested design yields a gain of 2.1, 5.7, 3.5, 3.5, 5.2 dBi and consistent radiation patterns at the working frequencies. The analysis of the diversity performance considers the Diversity Gain (DG) and Envelope Correlation Coefficient (ECC), whose values are near 9.9 dB and 0, respectively. Additionally, the assessed parameters are the CCL and TARC. The structure prototype has been developed, and the observed findings are highly coherent with the simulated results, making it appropriate for use in 5G NR bands, HIPERLAN, and IoT applications.

Keywords: Characteristic mode analysis; MIMO; Decoupling structure; IoT; ECC; Lower sub 6 GHz; HIPERLAN

NOMENCLATURE

DGS	: Defected ground structure
EBG	: Electromagnetic band gap
MIMO	: Multiple input multiple output
TCMA	: Theory of characteristic mode analysis
ECC	: Envelope correlation coefficient
DG	: Diversity gain
TARC	: Total active reflection coefficient
CCL	: Channel capacity loss

1. INTRODUCTION

To cope with the exponential increase of wireless traffic due to the increase in the use of numerous wireless applications besides Wi-Fi, it has led to the interference and congestion of the Wi-Fi frequency spectrum, reducing the quality of service. To meet the current wireless demands, a possible alternative is to deploy the network to another frequency band. 5G NR (new radio) bands were allocated, and a few bands above 6 GHz (unlicensed bands) were also analyzed and tested for 5G communications. All these paved the way for the development of MIMO systems in wireless devices, replacing the Single Input Single Output (SISO) technology drawbacks, such as multi-path fading, lower data rates, and the need for a broader frequency spectrum to accommodate high data rates. MIMO technology necessitates antennas with wide bandwidth and good isolation characteristics. It offers enhanced reliability, channel capacity, high quality, high data rate, fast communications with reduced interference, and can be used in all portable devices. So, the need of the hour is to develop a multi-functional, highly isolated, low-profile compact antenna structure suited for lower 5G NR (sub 6 GHz) and HIPERLAN/IoT applications.

In the literature, researchers provided a variety of techniques for improving the isolation between dual-band MIMO antennas. Parasitic elements, neutralisation lines, Electromagnetic Band Gap (EBG) structures, Defective Ground (DGS) techniques, decoupling networks, and characteristic mode analysis constitute some of the different isolation enhancement approaches. For increased isolation, various decoupling techniques[1-6] are used in MIMO antennas suited and designed for 5G applications. In[7-8] a decoupling structure was used for enhanced isolation of -40 and -25 dB suited for sub 6 GHz frequency applications connected between the radiators for enhanced isolation. In[10] isolation was improved (-24 dB) using a metamaterial superstrate patch sandwiched between the phased array elements. A neutralisation line and metamaterial loaded technique[11] was used for obtaining low mutual coupling array antenna. Interconnected/reduced/stepped ground plane[12-15] for enhancing isolation in MIMO antennas was used suited for 5G frequency bands. Parasitic elements[16] were used for mutual coupling reduction suited for LTE and Wi-Fi systems. The concept of CMA[17-18] (analysis of modes and modal significance) was used to improve the MIMO

Received : 19 December 2023, Revised : 30 March 2024
Accepted : 18 April 2024, Online published : 19 September 2024

performance. The antenna elements are triggered using various characteristic modes[19-20], and different characteristic currents are obtained, which enhanced the isolation. The concept of orthogonality[21] properties of characteristic modes was used for achieving good isolation. The DGS[22] concept was used to design a spiral antenna. The concept of neutralisation line[23] was used to design a highly isolated flower shaped MIMO antenna for 5G NR and WLAN applications. Characteristic mode manipulation concept[24] was used along with rectangular spiral shaped stub and L shaped slot for designing a triband MIMO for low sub 6 GHz. The concept of CMA[25] was used for MIMO dipole pair suited for base station applications. However, significant limitations of the techniques mentioned above include the high optimization time, proper positioning of the decoupling structures/neutralisation line/parasitic elements, complexity of the structures, limitation in the frequency region of operation (due to congestion at lower sub 6 GHz because of increase in wireless traffic) for obtaining good isolation in the working bands.

The novelty of the proposed design is seen in developing the antenna structure systematically with the help of theory of characteristic modes (TCM) and use of a decoupling structure (wide slot + narrow slots) on the ground plane for enhancing the isolation at multi bands, while in most of the cited work's isolation has been enhanced just nearer to an acceptable value[6,13-17] using the techniques which required high optimisation time, being placement dependent, complexity. The design is obtained and optimised in step-by-step procedure by perturbing the conventional rectangular structure with slots on the patch and the ground plane governed by quarter wavelength resonance enhancing isolation at working bands.

Moreover, the current design meets four major things needed for present wireless communication MIMO systems (i.e.) multifunctional, multiband antenna which can be used to cover 4G/5G NR bands as well as 17 GHz band suited for HIPERLAN, IoT services to avoid the wireless traffic congestion in low sub 6 GHz, while in most of the literary works the antennas are designed only for a specific application[1-6,7-8], good Impedance Bandwidth (IBW), compact structure with negligible losses. Furthermore, the system is analysed in terms of its diversity performance. The work is organized into the following sections: The basics of the characteristic mode analysis are outlined in Section 2, Section 3 offers the antenna design using the CMA concept, Section 4 outlines the experimental results and MIMO parameters of the proposed design, and conclusions are made in Section 5. The performance of the existing work is compared with the previously reported works, as highlighted in Table 1.

The following are the key contributions/advantages of the suggested work,

- The designed antenna is analyzed using the TCMA in terms of characteristic angle, modal significance, and eigenvalues, providing a deeper physical insight into the design regarding resonance conditions.
- The designed antenna is of less size ($0.58\ \lambda_0 \times 0.35\ \lambda_0 \times 0.01\ \lambda_0\ mm^3$ with an optimum element separation of $0.05\ \lambda_0$ (λ_0 is the lowest frequency operating wavelength)), less complexity, easy to fabricate (using PCB) and validate, less cost (because of ease of availability of FR-4 and PEC materials for fabrication).
- Enhanced isolation characteristics are observed at the resonant bands 2.2/4.2/7.2/16/17.5 GHz with $|S_{12}|$ values 47, 45, 24, 29, 39 dB using a simple decoupling structure of less complexity in the ground plane.
- Good impedance matching (observed from return loss/ VSWR values) and broadband resonance are obtained at the higher frequencies (16-19.5 GHz).
- The proposed structure offers acceptable diversity performance in terms of ECC (close to zero), DG (9.99 dB), TARC (< -10 dB), and CCL (< 0.5 bits/sec/Hz).
- A gain of > 2 dBi with stable radiation patterns is observed for the proposed design.
- The structure is designed as a multi-functional antenna system that can be used for 5G NR bands and HIPERLAN/ IoT applications as it covers the higher frequency unlicensed bands. This helps improve service quality in the frequency bands used for wireless applications suffering from high wireless traffic and congestion.

2. THEORY OF CMA (CHARACTERISTIC MODE ANALYSIS)

The concept of CMA was suggested in 1965 by Garbacz[26], which provides physical insight into the antenna design using the characteristic modes. This can be applied to any arbitrary antenna design with any shape and requires no excitation[27]. The CMA modal dynamics is evaluated in terms of the following parameters, which include the generalized eigenvalue equation for characteristic modes expressed as, $X(J_n) = \lambda_n R(J_n)$ where, λ_n denotes eigenvalue, J_n signifies the eigenvector, R and X represents the real and imaginary Hermitian elements of the standardized impedance matrix $Z=R+jX$[28]. λ_n is the ratio of reactive power to radiative power and is dependent on frequency.

An eigenvalue of zero indicates that the mode is at resonant condition, and a value less than or greater than zero indicates the storage of capacitive and inductive energies[29]. The modal significance computed as $MS_n = \left|1/(1+j\lambda_n)\right|$ is another alternate representation of the normalized form of eigenvalue[30]. The MS scale spans from 0 to 1. An MS value of 0.7 to 1 indicates the presence of – 10 dB impedance bandwidth and resonance. The characteristic angle (θ) is another essential metric that may be expressed as $\theta = 180^\circ - \tan^{-1}(\lambda_n)$, and the resonance condition is indicated at the operating bands by an angle of 180°. An angle of less than or greater than 180° indicates that the generated modes at the desired bands are inductive and capacitive.

3. DESIGN OF DECOUPLING STRUCTURE BASED MIMO ANTENNA

3.1 Layout and Design Procedure

The following steps summarise the entire proposed antenna design process:

- For the proposed structure, the effect of various modes has been analyzed using metrics such as characteristic angle, modal significance, and eigenvalues
- Using the results of characteristic mode analysis, decoupling structure and etching slots on the radiator are

Table 1. Comparison to prior existing designs

Ref.	Antenna dimension (mm^2)	Methodology used	Reduction in isolation $\|S_{12}\|$ (dB)	Design complexity	No. of operating bands
[1]	$1.47\ \lambda_0 \times 1.47\ \lambda_0$	Transmission line based	30	Complex	1
[2]	$2.12\ \lambda_0 \times 2.12\ \lambda_0$	Decoupling	25	Complex	1
[3]	$2.35\ \lambda_0 \times 2.35\ \lambda_0$	Decoupling	24	Simple	1
[4]	$0.83\ \lambda_0 \times 1.25\ \lambda_0$	Meta surface-based decoupling	32	Simple	2
[5]	$1.16\ \lambda_0 \times 1.16\ \lambda_0$	Ceramic superstrate-based decoupling	30	Complex	1
[6]	$1.63\ \lambda_0 \times 0.81\ \lambda_0$	Decoupling	11.2	Moderate	2
[7]	$0.63\ \lambda_0 \times 0.49\ \lambda_0$	Decoupling	30	Moderate	1
[8]	$0.8\ \lambda_0 \times 0.97\ \lambda_0$	Decoupling	25	Complex	1
[9]	$0.72\ \lambda_0 \times 0.32\ \lambda_0$	Defected ground + neutralisation line	17	Moderate	1
[10]	$3.88\ \lambda_0 \times 1.94\ \lambda_0$	Metamaterial superstrate patch between radiating elements	24	Moderate	2
[11]	$1.5\ \lambda_0 \times 1.04\ \lambda_0$	Metamaterial	30	Moderate	1
[12]	$0.88\ \lambda_0 \times 0.8\ \lambda_0$	Inverted L monopole antenna	25	Moderate	1
[13]	$1.17\ \lambda_0 \times 1.35\ \lambda_0$	Spacing between the elements	16	Simple	2
[14]	$1.52\ \lambda_0 \times 0.76\ \lambda_0$	Rectangular slots (DGS)	13	Simple	1
[15]	$0.73\ \lambda_0 \times 0.36\ \lambda_0$	Rectangular slot etched out in ground plane	20	Moderate	2
[16]	$0.64\ \lambda_0 \times 0.32\ \lambda_0$	Orthogonal modes+ defected ground	15	Complex	2
[17]	$0.72\ \lambda_0 \times 0.36\ \lambda_0$	Nil	8	Complex	2
[18]	$0.35\ \lambda_0 \times 0.17\ \lambda_0$	Orthogonal structure	NR	Moderate	2
[20]	$0.4\ \lambda_0 \times 0.33\ \lambda_0$	Opposite edges	20	Moderate	UWB (2-9.5 GHz)
[23]	$0.46\ \lambda_0 \times 0.3\ \lambda_0$	Neutralisation line	50	Simple	1
[24]	$0.25\ \lambda_0 \times 0.21\ \lambda_0$	Rectangular spiral stub+ L shaped slot	18	Moderate	3
This work	$0.58\ \lambda_0 \times 0.35\ \lambda_0$	CMA+ simple decoupling structure	2.2 GHz- 47 4.2 GHz- 45 7.2 GHz- 24 16 GHz- 25 17.5 GHz- 39	Simple	5 (covering low sub 6 GHz bands + HIPERLAN/IoT bands)

NR-Not reported; λ_0 represents the operating wavelength at the lowest cut off frequency.

the significant factors in determining the antenna working frequencies

- The combination of open-ended wide slots and narrow slots enhanced the isolation at the working band, making it suitable for low sub 6 GHz and HIPERLAN/IoT applications.

Figure 2 shows the suggested configuration in front and rear view. The structure comprises two identical radiators with a simple decoupling structure consisting of a broad slot and two-minute slots carved in the underground plane made of perfect electric conducting material (PEC). The layout is etched on an FR-4 epoxy substrate of dimension L×W with dielectric constant (ε_r) value of 4.3, loss tangent (tan δ) value of 0.025 and 1.6 mm of substrate height. The arrangement has an overall dimension of $0.58\ \lambda_0 \times 0.35\ \lambda_0 \times 0.01\lambda_0\ mm^3$ with an optimum element separation of 0.05 λ_0 (λ_0 is the lowest frequency operating wavelength). The suggested MIMO structure's initial dimensions are determined using the rectangular microstrip patch antenna fundamental equation[23]. The design of a single antenna element started with the rectangular patch, followed by four iterations to obtain the required working band frequencies. The optimised results have been attained following several iterations of structural alteration. Table 2. shows the optimum design dimensions. The suggested arrangement is obtained in four evolution stages, as depicted in Fig. 1, with front (left side) and rear (right side) views. The design is analyzed and optimized using an electromagnetic 3D Computer Simulation Technology (CST) microwave studio.

Stage I conventional antenna design uses two rectangular patches with a complete underground plane etched on the rear side of the dielectric material. In this step, the structure is not perturbed with any slots. A microstrip line feed with an impedance of 50 Ω is connected at the lower end of the patch using a strip of dimension e × f mm^2 (3 × 10 mm^2). It resonates at 4/5/8/16/17.5 GHz. Since no slot is etched between the radiators, more electromagnetic energy is coupled from port 1 to port 2, leading to poor isolation. In the following steps, a partial I-shaped radiator is obtained by etching four slots on the patches top, bottom, and left and right sides. In stage II, two slots of size g×h mm^2 (5×5 mm^2) are etched towards the right side top and bottom of the patches, producing resonant frequencies at 2/4/8/16/17.5 GHz. The ground plane is now perturbed to enhance the mutual coupling starting with a simple decoupling structure consisting of the wide slot of dimension c×d mm^2 (3×32 mm^2) which causes the changes in the surface current distributions on the radiating patches. In stage III, the design is further modified by an etching slot of size i×j mm^2 (10×19 mm^2) on the right side of the patches, producing resonant frequencies at 2.2/4.2/7.2/16/17.5 GHz. Two narrow slots of dimension a×b mm^2 (1 × 23.6 mm^2) are carved on the ground plane causing the surface currents to get trapped in these slots to improve the isolation at operating frequencies. In stage IV, the design is modified to improve the reflection coefficient by etching another slot of size k × l mm^2 (15 × 25 mm^2) on the left side of the patches to obtain the required partial I-shaped radiator. To further enhance the mutual coupling, a combination of two narrow slots of dimension a×b mm^2 (1×23.6 mm^2) along with a wide slot of dimension c×d mm^2 (3×32 mm^2) are carved on the underground plane. In this step, the designed antenna is resonating at pentaband frequencies 2.2/4.2/7.2/16/17.5 GHz with $|S_{11}| < -10$ dB, and an enhanced isolation of $|S_{12}| < -29$ dB was obtained compared to the prior evolution stage III and is suited for use in lower sub 6 GHz and HIPERLAN. Figure 3 displays the simulated isolation and return loss values for different design stages.

Table 2. MIMO structure dimensions

Parameters	Size (mm)
L/W	80/47.6
a/b/c/d/e/f/g/h/i/j/k/l/m/n/o	1/23.6/3/32/3/10/5/5/10/19/15/25/ 30/35/7

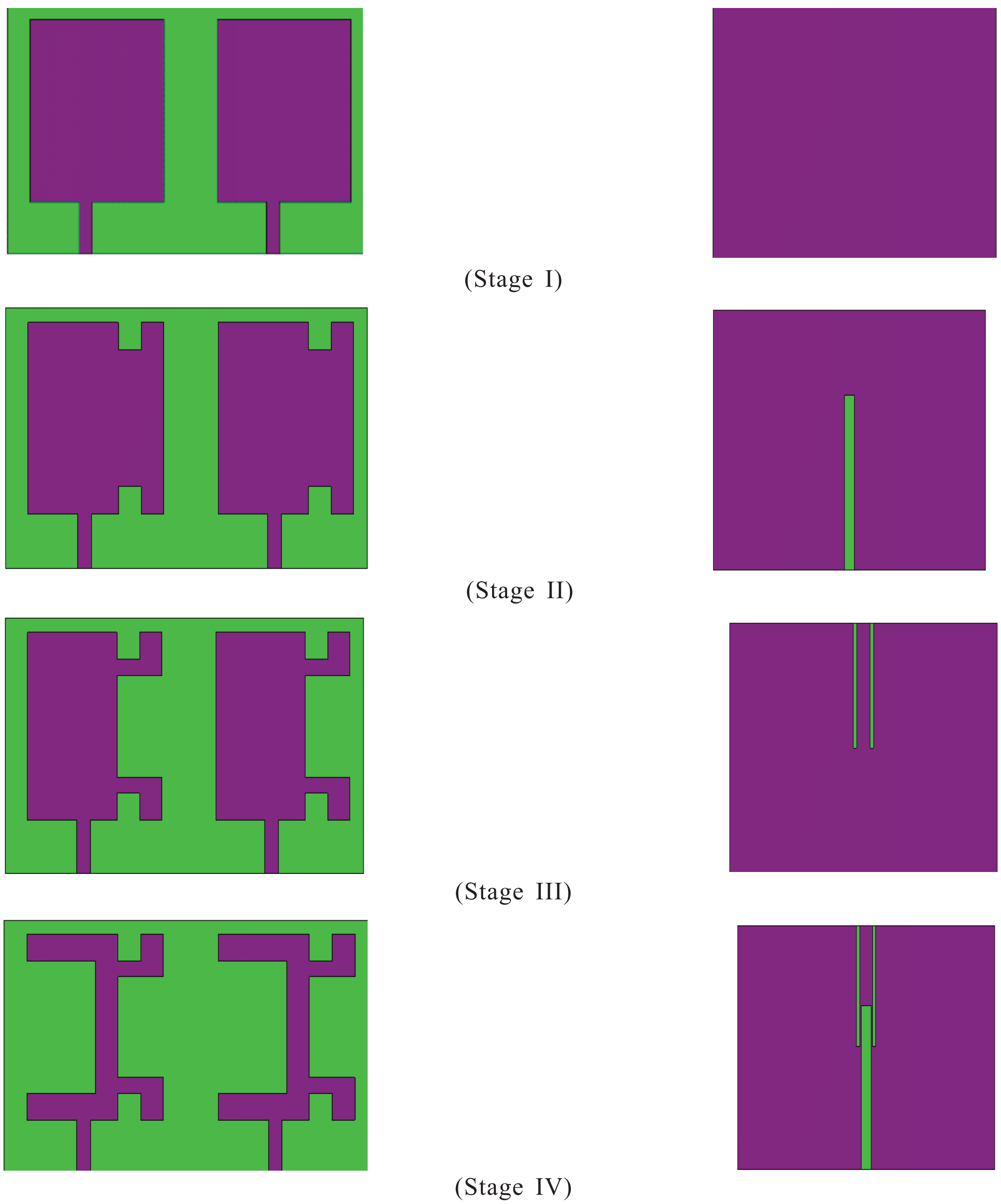

Figure 1. Design stages of the suggested structure (front/rear views).

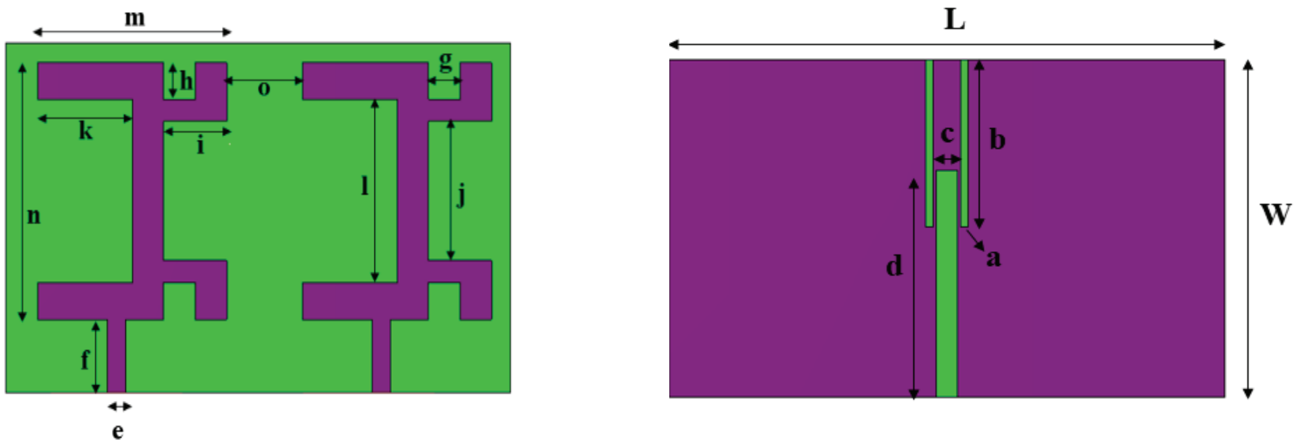

Figure 2. Front/ rear view geometry of the suggested structure.

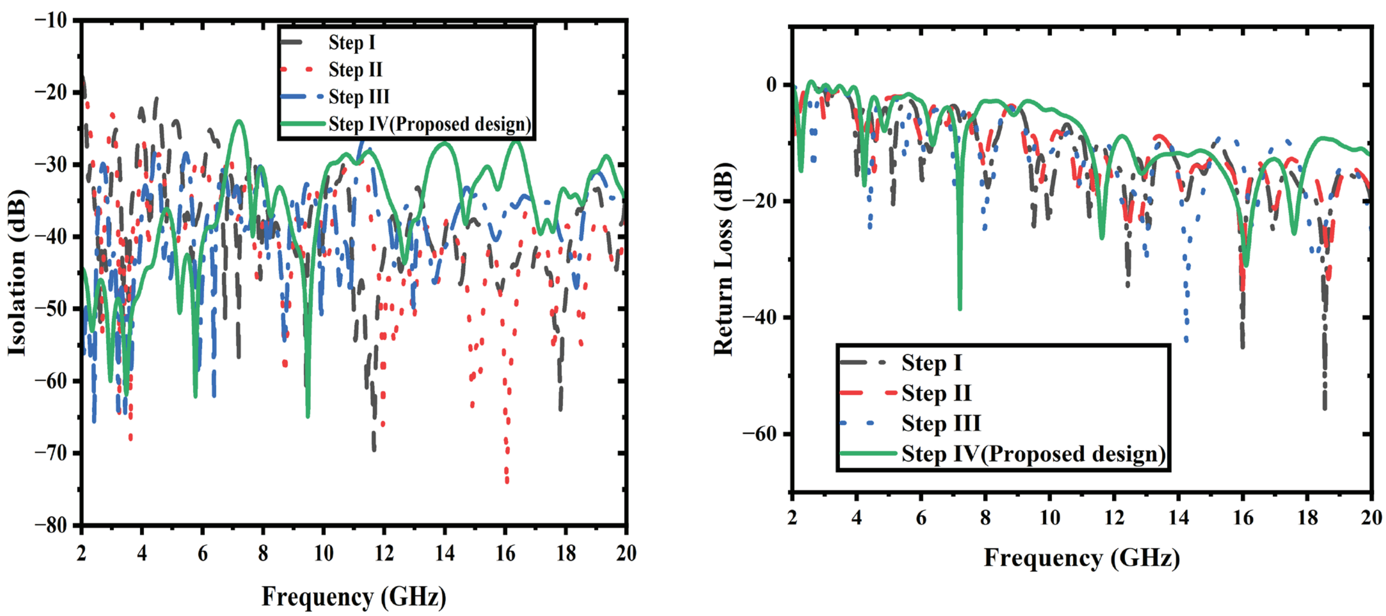

Figure 3. Simulated |S| parameter values for different stages of the suggested configuration.

3.2 Surface Current Distributions

For the proposed multi-functional radiator resonating at 2.2/4.2/7.2/16/17.5 GHz, surface current distributions are outlined in Fig. 4. The flow of surface currents is analysed on the suggested structure when port one is excited, and port two has a characteristic impedance termination of 50 Ω due to the symmetrical design. To gain better insight into the isolation mechanism, surface current distributions are analyzed at the resonant frequencies. In the absence of slots in the underground plane (stage I), there is no perturbation, and a high amount of EM energy is coupled between the ports, leading to poor mutual coupling as high surface currents are observed to be circulated by the feed line and the patch (left-sided) when port 1 is excited. In the later phases, the introduction of slot based simple decoupling structure consisting of a broad slot and a pair of minute slots created perturbations in the ground plane causing the surface current to get trapped in these slots producing an isolation of 47/45/24/25/29 dB at the working bands. The slot-based structure prevents the circulation of surface currents from radiators and also extends the path between the two radiators mitigating and diminishing the isolation effect.

3.3 Effect of Varying the Distance Between Patches

The structure is further examined by altering the distance (o) parameter between the patches, as the distance significantly impacts the mutual coupling of the designed antenna. The structure is analyzed for different values of o=4 to 8 mm with incremental values of 1 mm and return loss, mutual coupling values are observed at the desired operating frequencies, keeping the remaining structural parameters constant. The values of $|S_{11}|$ and $|S_{12}|$ obtained for different values of 'o' are compared as shown in Fig. 5, and the best-optimized dimension of o=7 mm has been chosen for the suggested antenna as it is observed that shift in the downward direction is more when o=7 mm compared to other values of 'o' suited for sub 6 GHz and HIPERLAN/IoT applications.

3.4 Design Using Characteristic Modes

The proposed penta band structure is analysed using an integral equation solver in computer simulation technology (CST) 2019 without giving the feed excitation. Figure 6(a) depicts the characteristic angle of the antenna for three distinct modes. From the graph, it is evident that mode 1 possesses an angle of 180° (indicating the resonance) at 2.2/4.2/7.2/16/17.5

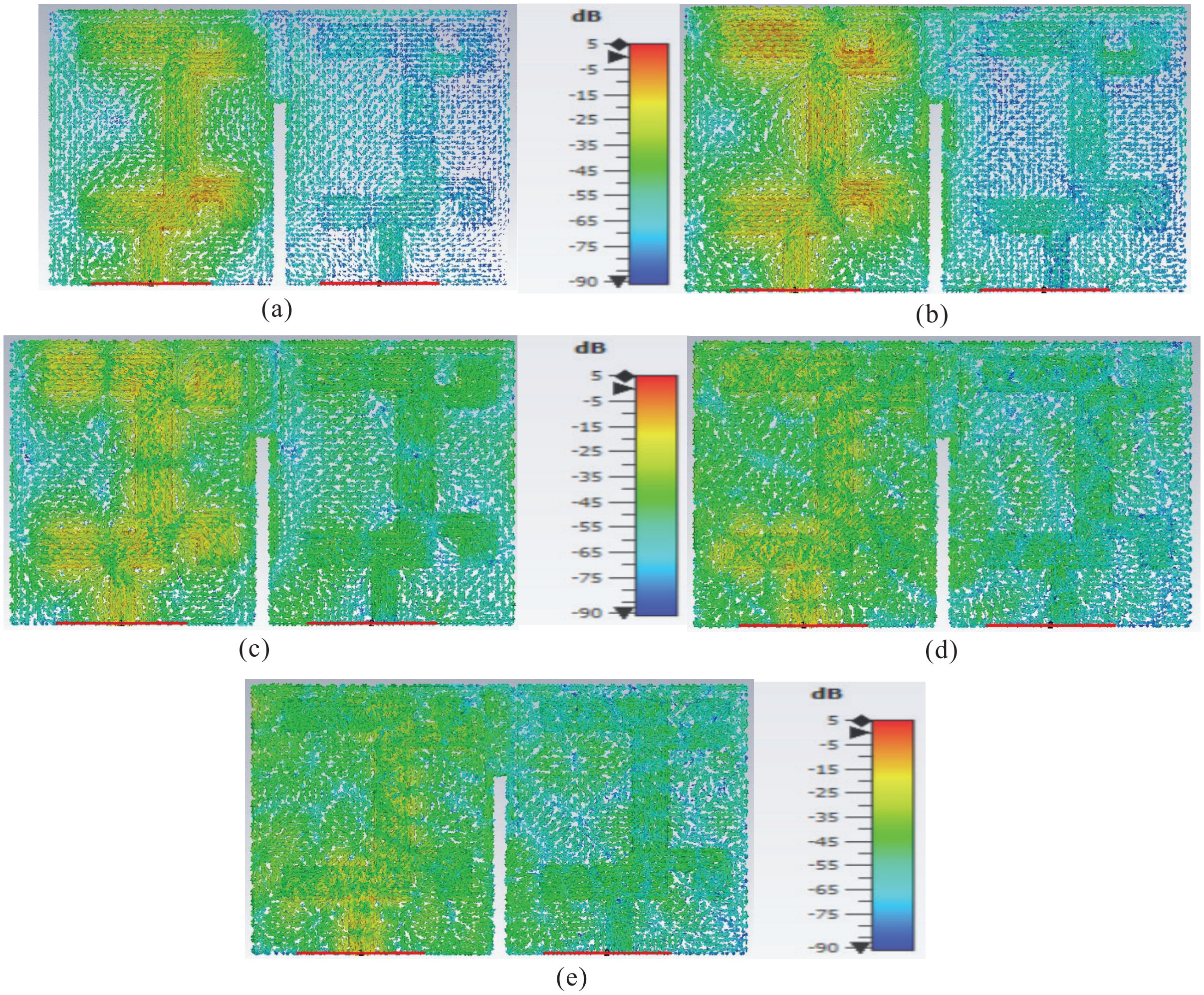

Figure 4. Surface current flow of the penta band structure, (a) At 2.2 GHz, port one is activated; (b) At 4.2 GHz, port one is activated; (c) At 7.2 GHz, port one is activated; (d) At 16 GHz, port one is activated; and (e) At 17.5 GHz, port one is activated.

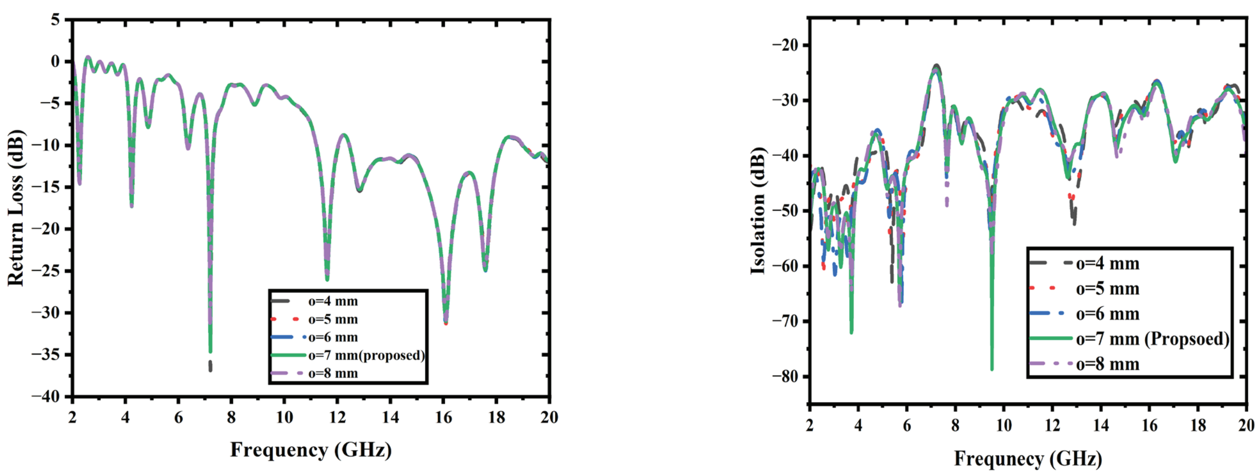

Figure 5. Simulated return loss/isolation values for various distance between the patches.

GHz frequencies. From this parameter, how much energy is stored can be determined at the desired frequencies. A <180° or > 180° angle indicates energy storage in the form of a magnetic/ electric field. Figure 6(b) illustrates the eigenvalue of the structure for three different modes. From the graph, it is evident that mode 1, being dominant, possesses EV close to zero at the desired frequencies, indicating resonance. An EV of < 0 or > 0 indicates the capacitive and inductive energies (which indicate more reactive power than radiated power). Figure 6(c) represents the MS parameter of the design analyzed using three modes; from the graph, only mode 1 has an MS value of 1 at the frequencies 2.2/4.2/7.2/16/17.5 GHz, while mode 2 and mode 3 have MS value of 1 at some other frequencies. Mode 1 is considered to be dominant for the designed antenna.

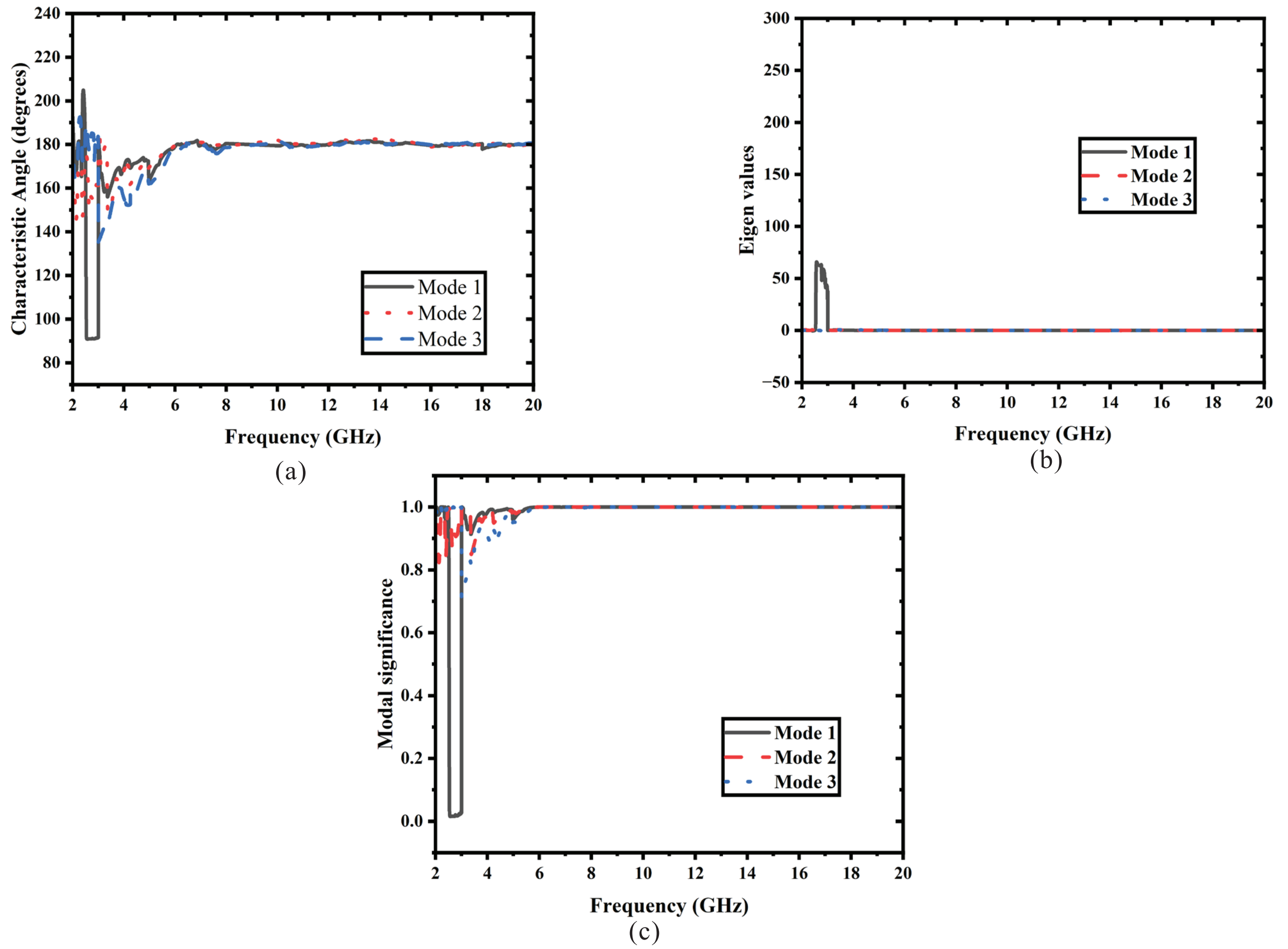

Figure 6. CMA of the penta band structure.

Table 3. CMA (mode 1) of the suggested MIMO structure

Frequency (GHz)	Modal significance	Characteristic angle (in degrees)	Eigen value
2.2	0.999	179.8	0.003
4.2	0.991	172.6	0.12
7.2	0.999	180	0
16	0.999	179.5	0
17.5	0.999	180	0

Table 3 shows the CMA values for mode 1 of the suggested MIMO structure.

4. EXPERIMENTAL RESULT ANALYSIS

4.1 |*S*| Parameters and Impedance Bandwidth

The proposed arrangement is developed and verified using the simulated results, as displayed in Fig. 7, and measurements are performed using a VNA (Anritsu MS2037C). The MIMO antenna designed is symmetrical in nature so the response for both the ports is almost same if excited from port 1 or port 2. Figure 8 outlines the simulated and measured findings of |*S*| parameters at the desired frequencies 2.2/4.2/7.2/16/17.5 GHz. The simulated and measured $|S_{11}|$ values are <15 dB at the resonant frequencies. The isolation is enhanced by employing a simple decoupling arrangement consisting of a broad slot and a pair of minute slots and adequately tuning the

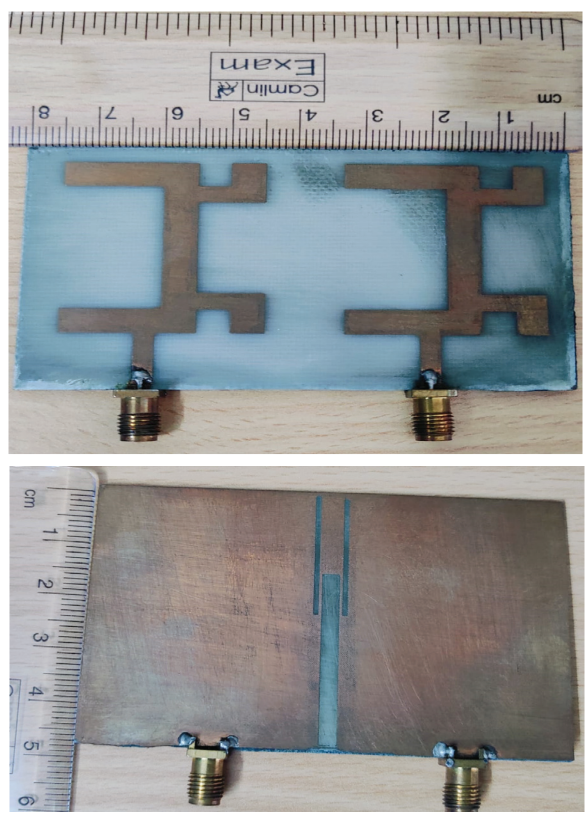

Figure 7. Geometry of fabricated structure.

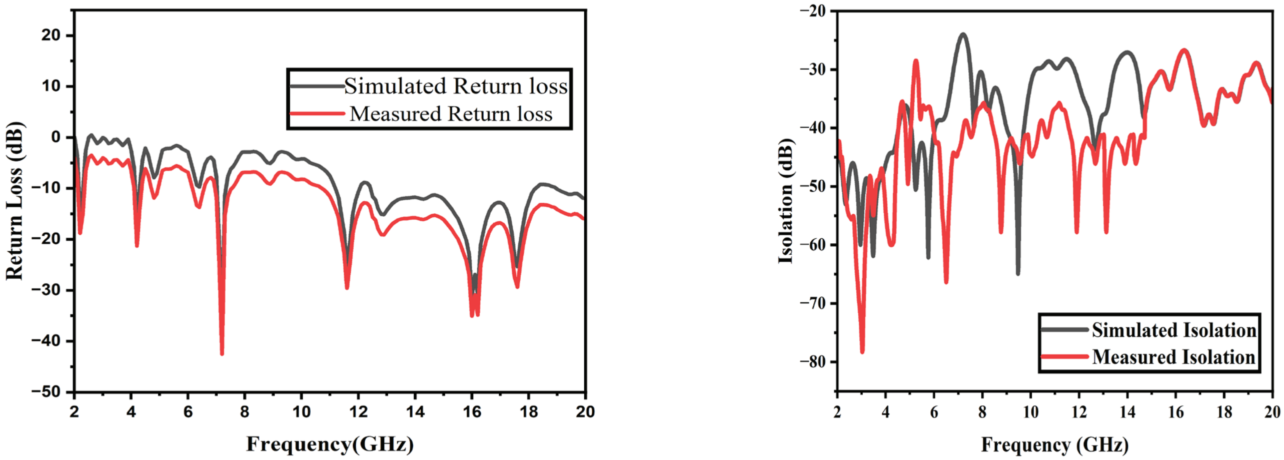

Figure 8. Simulated/validated |S| parameters of the suggested antenna structure.

modes produced $|S_{12}|$ values as 47, 45, 24, 25, and 39 dB at the resonant frequencies. A slight variance is observed between simulated and actual findings due to the SMA connector losses, improper calibration, errors in soldering, and other losses. The measured -10 dB impedance bandwidths are around 0.2, 0.2, 0.38, 3.6, and 2 GHz at the operating frequencies.

4.2 Radiation Pattern Characteristics

Figure 9(i-v) indicates the antenna modeled and measured co and cross polarisation for constant phi (varying theta at 0°, 90°) and constant theta (varying phi at 0°, 90°) at 2.2/4.2/7.2/16/17.5 GHz measured at one antenna. At the same time, the other has a 50 Ω characteristic impedance termination. The pattern is almost omnidirectional at a lower sub-6 GHz frequency of 2.2 GHz. At 4.2 GHz, it is distorted omnidirectional. The pattern is almost distorted dumbbell-shaped in the high frequency region of 7.2/16/17.5 GHz. This variation in the radiation patterns at low and high frequencies can be attributed to antenna radiation patterns depending on the antenna dimensions with respect to wavelength. A little bit distortion in characteristics is observed which can be attributed to design parameters of both the antenna and DGS. The shape and location of lobes, nulls are influenced by the DGS causing the pattern to change its characteristics. The antenna directivity is measured based on the values of its radiation pattern.

The setup includes an anechoic chamber that minimizes reflections and external interference controlled by the environment. The antenna Under Test (AUT) is mounted for precise rotation and positioning of the measurement system. The setup procedure to measure the directivity of the antenna is prepared. The ratio of maximum radiation intensity in the desired direction to the radiation intensity averaged in overall directions is measured with respect to the reference antenna, which is a horn antenna. Fig. 10 shows the proposed antenna directivity at the desired frequencies, and Fig. 10 (right side graph) shows the proposed antenna gain at operating frequencies, which are 2.1, 5.7, 3.5, 3.5, 5.2 dBi at the operating frequencies. The accuracy of the findings is primarily determined by using standard measurement set up involving the proper handling of the motor movements for rotating the AUT, the impact of the probe being used, the effect of RF connectors, the interconnection between different systems, the movement of RF cables, and a reflection-free anechoic chamber environment. Nevertheless, as can be shown in Fig. 9, 10, only a little divergence results because of the accurate handling of the aforementioned factors.

4.3 Diversity Performance

The diversity parameters of the designed multi-functional antenna are analyzed in terms of two major parameters: envelope correlation coefficient (ECC) and diversity gain (DG). Figure 11(a) and 11(b) depict ECC and DG's simulated and validated values. At the operating frequencies, the obtained ECC values are close to zero, which can be found using the

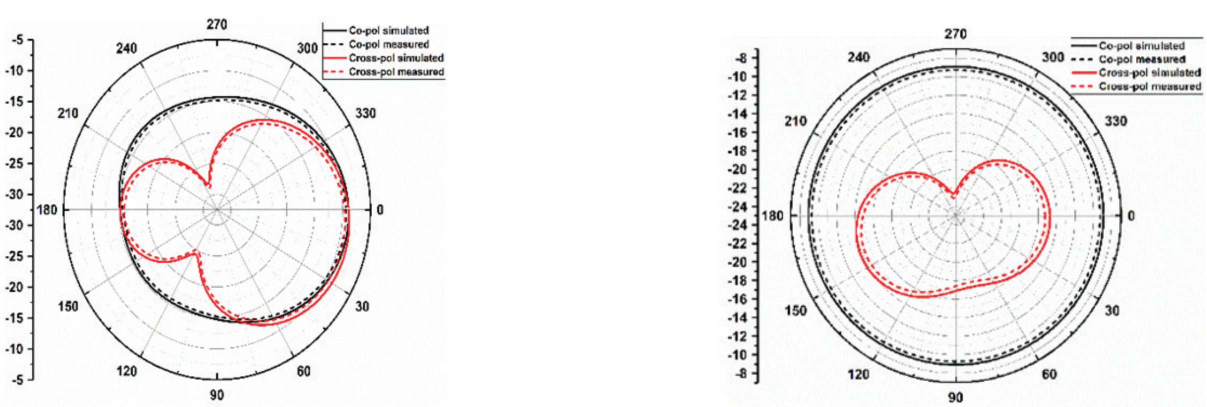

E-Plane 2.2 GHz (i) H-Plane 2.2 GHz

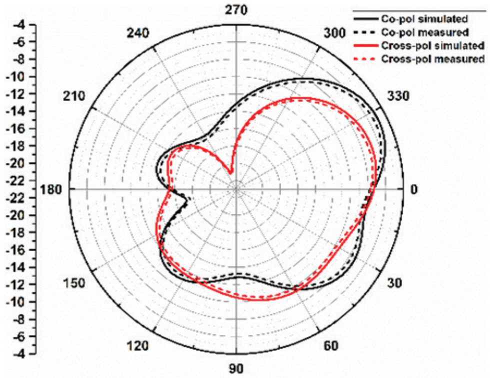

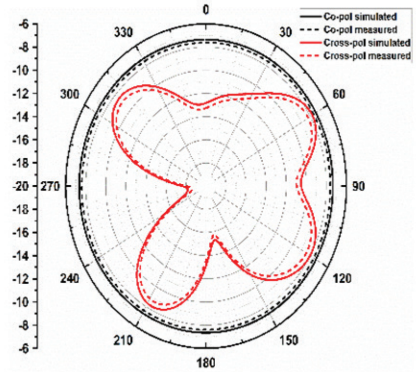

E-Plane 4.23 GHz (ii) H-Plane 4.23 GHz

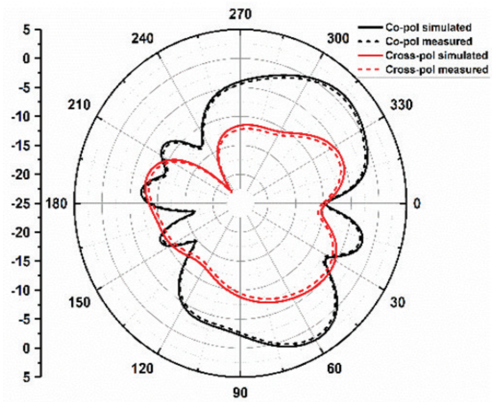

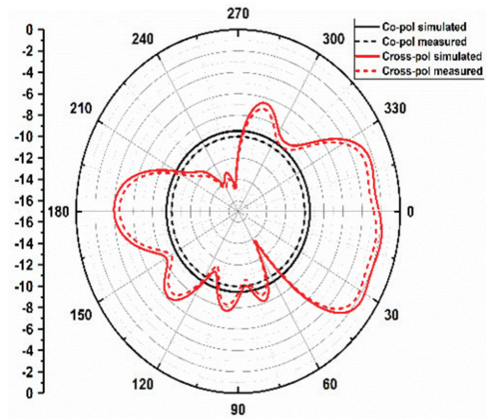

E-Plane 7.2 GHz (iii) H-Plane 7.2 GHz

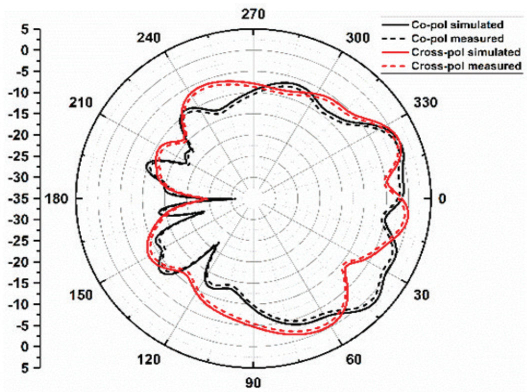

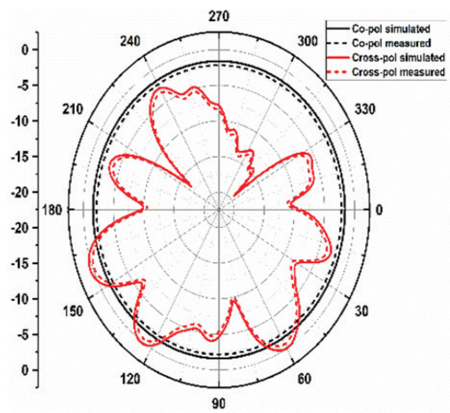

E-Plane 16 GHz (iv) H-Plane 16 GHz

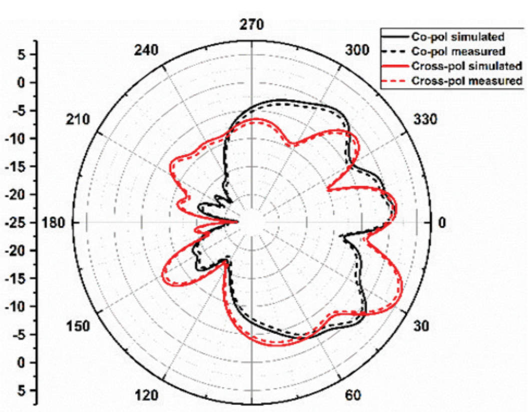

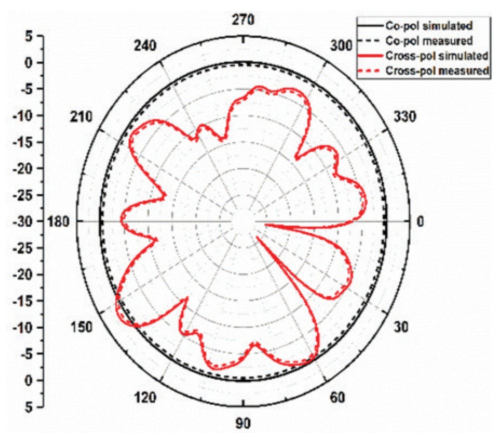

E-Plane 17.5 GHz (v) H-Plane 17.5 GHz

Figure 9. (i-v) Radiation patterns (E-field and H-field) of MIMO antenna structure at 2.2/4.2/7.2/16/17.5 GHz.

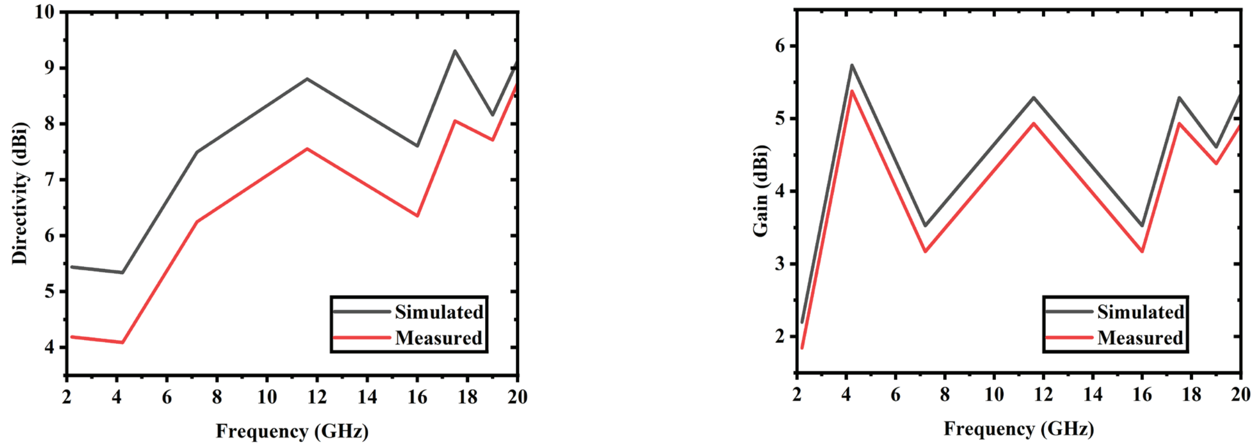

Figure 10. Diversity/Gain of proposed structure.

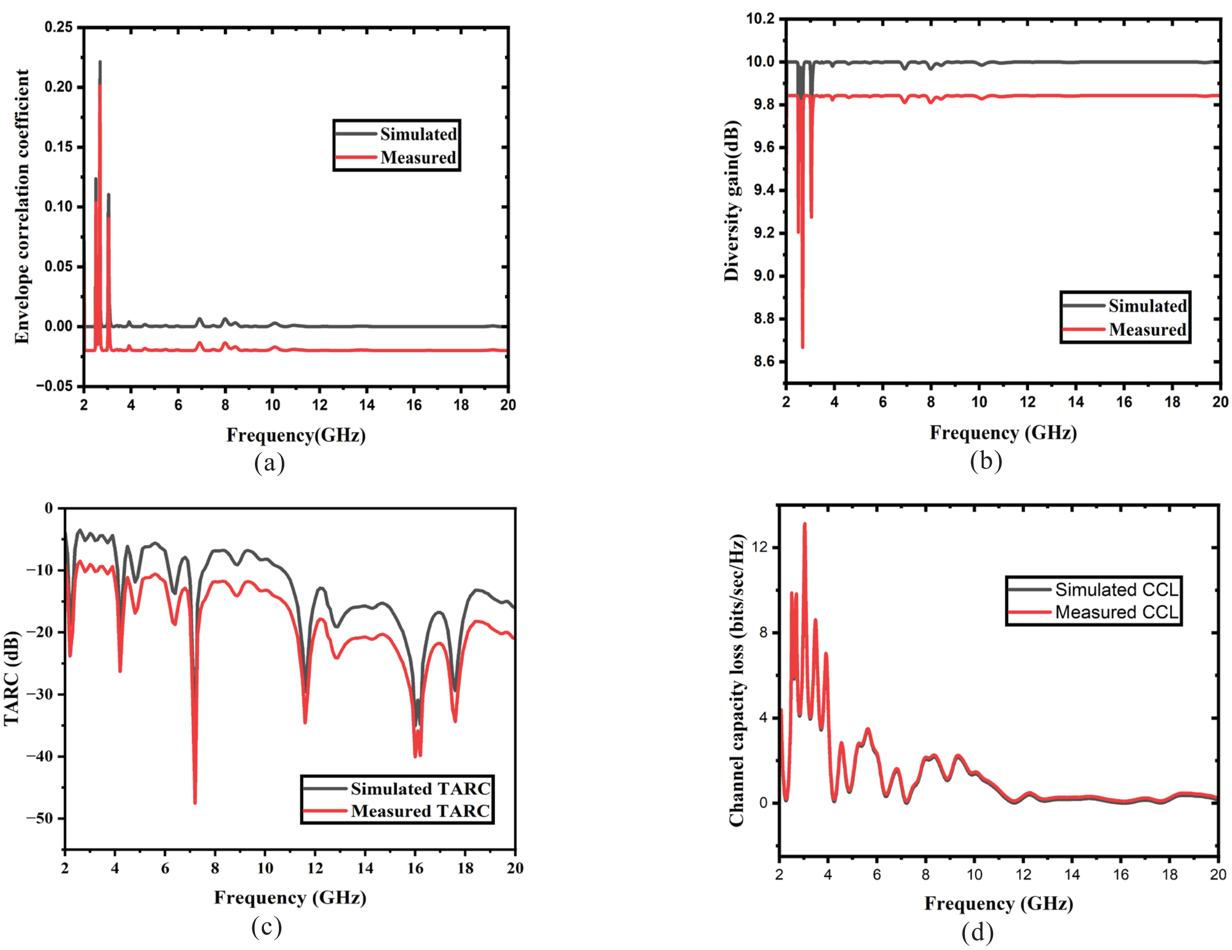

Figure 11. ECC/DG/TARC/CCL of proposed structure.

following equation for a 2×1 MIMO system[20].

$$\rho = \frac{\left|S_{11}^{*} \times S_{12} + S_{21}^{*} \times S_{22}\right|^2}{\left(1-\left(\left|S_{11}\right|^2+\left|S_{21}\right|^2\right)\right)\left(1-\left(\left|S_{22}\right|^2+\left|S_{12}\right|^2\right)\right)} \quad (1)$$

The DG values are around 9.99 dB at the resonant frequencies, which can be computed using equation[20]. A low ECC value and a high DG value indicate the proposed structure has superior diversity performance.

$$DG = 10\sqrt{1-\left|\rho\right|^2} \quad (2)$$

The other assessed parameter is the total active reflection coefficient (TARC), computed from |*S*| parameters for a 2×1 MIMO antenna system using the following equation[12]. At the resonant frequencies, the values of TARC are < -10 dB, which can be observed from Fig 11c.

$$TARC = \sqrt{\frac{\left|S_{11} + S_{12}e^{j\theta}\right|^2 + \left|S_{21} + S_{22}e^{j\theta}\right|^2}{2}} \tag{3}$$

where, θ is the phase, whose value varies from 0(0°) to 2ø (360°).

The channel capacity provides how much bandwidth the channel can take and accept without losses. The Shannon capacity A for the MIMO system is computed by employing the following formula[9] based on the channel matrix, H.

$$A = \log_2\left(\det\left(1 + \frac{SNR}{M}HH^{'}\right)\right) \tag{4}$$

where, SNR is the expected channel signal to noise ratio, M is the number of receivers, and H' is the Hermitian of the matrix H. The following formulae can be used to determine the channel capacity loss for a MIMO[9].

$$C_{Loss} = -\log\left(\det\left(\psi^R\right)\right) \tag{5}$$

where

$$\psi^R = \begin{pmatrix} \rho_{1,1} & \cdots & \rho_{1,N} \\ \vdots & \ddots & \vdots \\ \rho_{N,1} & \cdots & \rho_{N,N} \end{pmatrix}$$

$$\psi^R = \begin{pmatrix} \rho_{11} & \rho_{12} \\ \rho_{21} & \rho_{22} \end{pmatrix}$$

$$\rho_{ii} = 1 - \left(\left|S^2{}_{ii}\right| - \left|S_{ij}{}^2\right|\right)$$

$$\rho_{ij} = -\left(S_{ii}{}^* S_{ij} + S_{ij}{}^* S_{jj}\right)$$

for i, j = 1 or 2.

At the working bands the obtained CCL values are < 0.4 bits/s/Hz which are within the acceptable values ensuring good throughput and low losses. However, exceeding the limits in the non-working band is due to unacceptable values of |S| parameters (at those non-working frequencies), as CCL is solely determined by |S| parameters, as shown in Fig. 11(d). As can be seen, all of the suggested MIMO system parameters are well within acceptable ranges, making it a potential device for use in 5G NR bands and HIPERLAN, IoT applications.

5. CONCLUSIONS

The article outlines a penta band novel compact MIMO configuration using CMA to cover 5G NR bands at 2.2, 4.2, 7.2 GHz and HIPERLAN, IoT 16, and 17.5 GHz applications. The design is investigated based on TCMA regarding characteristic angle, modal significance, and eigenvalues. A partial I-shaped MIMO radiator is proposed with an average enhanced isolation of < -25 dB by using a simple decoupling structure consisting of broad slot and two-minute slots in the underground plane and adequately tuning the modes. The MIMO diversity parameters are also assessed and presented, which show that the suggested antenna can be used in low sub 6 GHz and HIPERLAN/IoT applications. The observed and simulated findings are consistent.

REFERENCES

1. Zhang, Y.M.; Zhang, S.; Li, J.L. & Pedersen, G.F. A transmission-line-based decoupling method for MIMO antenna arrays. *IEEE Trans. Antennas Propag.*, 2019, **67**(5), 3117-3131.
doi:10.1109/TAP.2019.2900406
2. Tang, J. & Faraz, F.; Chen, X.; Zhang, Q.; Li, Q.; Li, Y. & Zhang, S. A meta surface Superstrate for mutual coupling reduction of large antenna arrays. *IEEE Access.*, 2020, **8**, 126859-126867.
doi: 10.1109/ACCESS.2020.3008162.
3. Luo, S.; Pedersen G.F. & Zhang, S. Massive MIMO array design with high isolation by using decoupling cavity. *IEEE Trans. Circuits Syst. II: Express Briefs.*, 2023, **70**(3), 974-978.
doi: 10.1109/TCSII.2022.3216394.
4. Liu, F.; Guo, J.; Zhao, L.; Huang, G.-L.; Li, Y. & Yin, Y. Dual-band meta surface-based decoupling method for two closely packed dual-band antennas. *IEEE Trans. Antennas Propag.*, 2020, **68**(1), 552-557.
doi: 10.1109/TAP.2019.2940316.
5. Liu, F.; Guo, J.; Zhao, L.; Huang, G. L.; Li, Y. & Yin, Y. Ceramic superstrate-based decoupling method for two closely packed antennas with cross-polarization suppression. *IEEE Trans. Antennas Propag.*, 2021, **69**(3), 1751-1756.
doi: 10.1109/TAP.2020.3016388.
6. Li, J. & Zhang, X.; Wang, Z.; Chen, X.; Chen, J.; Li, Y. & Zhang, A. Dual-band eight-antenna array design for MIMO applications in 5G mobile terminals. *IEEE Access.*, 2019, **7**, 71636-71644.
doi: 10.1109/ACCESS.2019.2908969.
7. Chen, S.C.; Wang, Y.-S. & Chung, S.J. A decoupling technique for increasing the port isolation between two strongly coupled antennas. *IEEE Trans. Antennas Propag.*, 2008, **56**(12), 3650-3658.
doi: 10.1109/TAP.2008.2005469.
8. Liu, F.; Guo, J.; Zhao, L.; Shen, X. & Yin, Y. A meta-surface decoupling method for two linear polarized antenna array in Sub-6 GHz base station applications. *IEEE Access.,* 2019, **7**, 2759-2768.
doi: 10.1109/ACCESS.2018.2886641.
9. See, C.H.; Abd-Alhameed, R.A.; Abidin, Z.Z.; McEwan, N.J. & Excell, P.S. Wideband printed MIMO/Diversity monopole antenna for Wi-Fi/WiMAX applications. *IEEE Trans. Antennas Propag.*, 2012, **60**(4), 2028-2035.
doi: 10.1109/TAP.2012.2186247.
10. Alibakhshikenari, M. Salvucci, A.; Polli, G.; Virdee, B.S.; See, C.h.; Abd-Alhame, R.; Falcone, F.; Andújar, A.; Anguera, J. & Limiti, E. Mutual coupling reduction using metamaterial super substrate for high performance & densely packed planar phased arrays. 22nd International Microwave and Radar Conference (MIKON), Poznan, Poland, 2018.
doi: 10.23919/MIKON.2018.8405323.
11. Luo, Shengyuan; Li, Yingsong; Xia, Yinfeng & Zhang, Liang. A low mutual coupling antenna array with gain enhancement using metamaterial loading and neutralization line structure. *ACES J.*, 2019, **34**(3), 411-418.https://journals.riverpublishers.com/index.php/

ACES/article/view/8555 (Accessed on 6 November 2023)

12. Sarkar, D. & Srivastava, K.V. A compact four-element MIMO/Diversity antenna with enhanced bandwidth. *IEEE Antennas Wirel. Propag. Lett*., 2017, **16**, 2469-2472.
doi: 10.1109/LAWP.2017.2724439.
13. Talha, M.Y.; Babu, K.J. & Aldhaheri, R.W. Design of a compact MIMO antenna system with reduced mutual coupling. *Int. J. Microwave Wireless Technol.*, 2016, **8**(1), 117-124.
doi: 10.1017/S1759078714001287
14. Chouhan, S. & Malviya, L. Four-port shared rectangular radiator with defected ground for wireless application. *Int. J. Commun. Syst.,* 2020, **33**(9), e4356.
doi: 10.1002/dac.4356
15. Chattha, H.T. Compact high isolation wideband 4G and 5G multi-input multi-output antenna system for handheld and internet of things applications. *Int. J. RF Microw. Comput. Aided Eng.*, 2019, **29**(6), e21710.
doi: 10.1002/mmce.21710
16. Moradikordalivand, A.; Leow, C.Y.; Rahman, T.A.; Ebrahimi, S. & Chua, T.H. Wideband MIMO antenna system with dual polarization for Wi-Fi and LTE applications. *Int. J. Microwave Wireless Technol.*, 2016, **8**(3), 643-650.
doi:10.1017/S175907871500032X
17. Ghalib, A.; Hussain, R. & Sharawi, M.S. Analysis of slot-based radiators using TCM and its application in MIMO antennas. *Int. J. RF Microw. Comput. Aided Eng.*, 2019, **29**(2), e21544.
doi: 10.1002/mmce.21544
18. Miers, Z.; Li, H. & Lau, B.K. Design of bandwidth-enhanced and multiband MIMO antennas using characteristic modes. *IEEE Antennas Wirel. Propag. Lett*., 2013, **12**, 1696-1699.
doi:10.1109/LAWP.2013.2292562
19. Hamad; E.K.I. & Ahmed, A. Metamaterial superstrate microstrip patch antenna for 5G wireless communication based on the theory of characteristic modes. *J. Electr. Eng.,* 2019, **70**(3), 187-197.
doi: 10.2478/jee-2019-0027
20. Zhao, X.; Yeo, S.P. & Ong, L.C. Planar UWB MIMO antenna with pattern diversity and isolation improvement for mobile platform based on the theory of characteristic modes. *IEEE Trans. Antennas Propag.*, 2018, **66**(1), 420-425.
doi: 10.1109/TAP.2017.2768083.
21. Saraswat, K. & Harish, A.R. Analysis of wideband circularly polarized ring slot antenna using characteristics mode for bandwidth enhancement. *Int. J. RF Microw. Comput. Aided Eng.*, 2018, 28(2), e21186.
doi: 10.1002/mmce.21186
22. Ahirwar, S.; Rao, A. & Chakravarthy, M. Design of a low-profile archimedean spiral antenna using compact defected ground structure as a reflector. *Def. Sci. J.*, 2023, **73**(5), 572-581.
doi: 10.14429/dsj.73.17751
23. Babu, K.V.; Das, S.; Ali, S.S.; Ghzaoui, M.; Madhav, B.T.P. & Patel, K.S. Broadband sub-6 GHz flower-shaped MIMO antenna with high isolation using theory of characteristic mode analysis (TCMA) for 5G NR bands and WLAN applications. *Int. J. Commun. Syst.,*2023, **36**(6), e5442. doi:10.1002/dac.5442
24. Xia, Cao.; Yingqing, Xia.; Ling, W. & Xiaolin, Wu. Tri-band MIMO antenna design based on characteristic modes manipulation. *AEU-Int. J. Electron. Commun.,* 2022, 155, 154318.
doi: 10.1016/j.aeue.2022.154318
25. Li, M. & Xiao, B.; Zhou, C.; Wu, D.; Yeung, K.L.; Jiang, L. & Murch, R. Novel CMA scheme to design self-decoupled MIMO dipole pair for base-station applications. *IEEE Trans. Antennas Propag.*, 2022, **70**(4), 2480-2489.
doi: 10.1109/TAP.2021.3118812.
26. Garbacz, R.J. Modal expansions for resonance scattering phenomena. *Proceedings of the IEEE*., 1965, **53**(8), 856-864.
doi: 10.1109/PROC.1965.4064
27. Harrington, R. & Mautz, J. Computation of characteristic modes for conducting bodies. *IEEE Trans. Antennas Propag.*, 1971, **19**(5), 629-639.
doi:10.1109/TAP.1971.1139990
28. Cabedo Fabrés, M. Systematic design of antennas using the theory of characteristic modes. Universitat Politècnica de València, 2008. (PhD Thesis).
doi: 10.4995/Thesis/10251/1883
29. Newman, E. Small antenna location synthesis using characteristic modes. *IEEE Trans. Antennas Propag.*, 1979, **27**(4), 530-531.
doi: 10.1109/TAP.1979.1142116.
30. Chen, Y. & Chao-Fu, W. Characteristic modes: Theory and applications in antenna engineering. Wiley Telecom, 2015.
doi: 10.1002/9781119038900.

CONTRIBUTORS

Ms Makkapati Himaja obtained her MTech degree in Digital Electronics and Communication Systems from VVIT, Guntur, Andhra Pradesh. Her areas of research are MIMO and filtennas, using the concept of defective ground structures and developing highly isolated MIMO antennas using TCMA concept, MIMO antennas with reduced RCS for electronic warfare applications, and filtennas for MIMO applications.
Contributions to the current study: Conceptualization, carrying out design, computer simulation studies, measurement analysis, data organization, and drafting of the manuscript.

Dr S. Yuvaraj obtained his PhD from IIT Roorkee, India. His areas of research include: Millimeter and THz wave sources and allied components, microwave/millimeter passive circuits, microwave sensors, and microwave/millimeter wave antennas. Contributions in the current study: Conceptualisation, reviewing the results and manuscript drafts, and overall work supervision.